

Title:

DESIGN AND OPERATION OF A BUTTON-PROBE,
BEAM-POSITION MEASUREMENTS

JUL 84

Author(s):

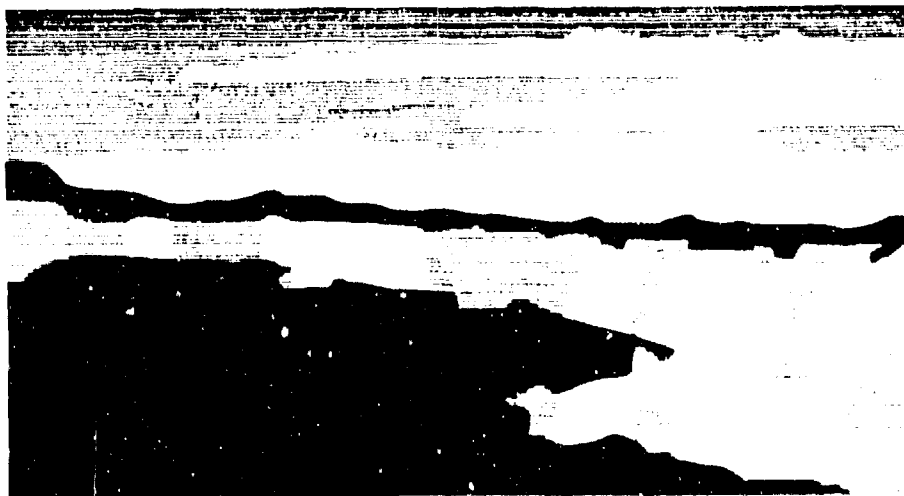
J. D. Gilpatrick
J. F. Power
R. E. Meyer
C. R. Rose

Submitted to:

1993 Particle Accelerator Conference
Washington, DC
May 17-20, 1993

MASTER

Los Alamos
NATIONAL LABORATORY



Design and Operation of Button-Probe, Beam-Position Measurements

J. D. Gilpatrick, J. F. Power, R. E. Meyer, and C. R. Rose
Los Alamos National Laboratory
Los Alamos, NM 87545

Abstract

Beam position measurement systems have been installed on the Advanced Free Electron Laser (AFEL) facility at Los Alamos National Laboratory [1]. The position measurement uses a capacitive- or button-style probe that differentiates the beam-bunch charge distribution induced on each of the four probe lobes. These induced signals are fed to amplitude-to-phase processing electronics that provide output signals proportional to the arc tangent of the probe's opposite-lobe, signal-voltage ratios. An associated computer system then digitizes and linearizes these processed signals based on theoretical models and measured responses. This paper will review the processing electronics and capacitive probe responses by deriving simple theoretical models and comparing these models to actual measured responses.

I. INTRODUCTION

The goal of the AFEL was to demonstrate that a free electron laser (FEL) suitable for industrial, medical, and research application can be built. This goal has been achieved by accelerating an electron beam to 20 MeV with a bunching frequency of 108.3 MHz and transporting the beam into and out of a FEL. To have sufficient lasing efficiency from this wiggler-based laser, the electron beam position and trajectory angle must be known at the entrance and exit of the wiggler with resolutions and accuracies of a few tenths of a percent and a few percent of the beam pipe radius, respectively. Also, this beam position information must be known over as few microbunches as possible while maintaining at least a factor of ten in beam current dynamic range. To attain these measurement goals, the preferred measurement system choice was an integrated beam-position measurement system similar to those implemented on the Ground Test Accelerator (GTA) [2]. The AFEL beam position and intensity measurements consist of three basic components: a capacitive- or button style probe, an amplitude-to-phase position processor, and associated linearization algorithms that reside in the control system.

Table 1

Specification of the AFEL Position and Intensity measurements

	Position	Intensity
Measurement Range	± 10 mm	460 to 1 A _{pk}
Dynamic Range (nC/bunch)	4.6 to 0.01	4.6 to 0.01
Resolution	± 25 μ m	± 1 A _{pk}
Accuracy	± 0.25 mm	± 10 A _{pk}
Bandwidth (MHz)	3.5	3.5

*Work supported by the US Department of Energy, Office of High Energy and Nuclear Physics.

Table 1 describes the specifications for the beam position and intensity measurement systems.

II. MEASUREMENT SYSTEM DESCRIPTION

Figure 1 shows a picture of the capacitive-style beam-position monitor (BPM) installed on the AFEL beamline. Each probe consists of four rectangular metal lobes whose dimensions are defined by the subtended lobe angle of 45° and a 3.2 mm length. The probe clear aperture is 2.34 cm with a lobe aperture of 2.54 cm. Alignment of the probe assembly with the accelerator beamline is achieved by using the four bosses located on the upstream probe vacuum flange (see Figure 1). These bosses are used in both a beamline alignment process and a probe taut-wire characterization fixture to find the absolute offsets and sensitivities to beam position. This alignment and probe characterization procedure provides sufficient information to make absolute beam position measurements to the nearest ± 0.25 mm.



Figure 1. The AFEL capacitive probe shown with its alignment stand and an associated coaxial transmission line.

The signal power from each lobe is calculated by assuming that the Gaussian distributed beam image charge on each probe lobe is

$$\rho(z,t) = \frac{q_0}{2\pi\sqrt{2\pi}\sigma} e^{-\frac{(z-z_0)^2}{2\sigma^2}} \quad (1)$$

where $\rho(z)$ is the beam charge distribution, eN is the total charge per bunch, θ_0 is the subtended angle of the probe lobe, σ is the bunch length, and βc is the beam velocity. The beam image current induced on each of the probe lobes, Equation (2), is the integral of $\rho(z)$ in the z -dimension and the time derivative where τ is the rms temporal bunch length,

$$i_B(t) = -\frac{eN\theta_0}{\sqrt{2\pi\tau}} \left[e^{-\frac{t^2}{2\tau^2}} - e^{-\frac{(t-L/\beta c)^2}{2\tau^2}} \right] \quad (2)$$

and L is the length of the lobe. The beam-induced output voltage, $V_P(j\omega)$, at the input to the processing electronics is

$$V_P(j\omega) = \frac{\sigma(j\omega)I_B(j\omega)}{\sqrt{2}} \frac{Z_c}{1+j\omega Z_c C_P} \frac{1}{I_0\left(\frac{\omega R}{\beta c}\right)} \frac{2I_1\left(\frac{\omega r}{\beta c}\right)}{\left(\frac{\omega r}{\beta c}\right)}, \quad (3)$$

where C_P is the probe capacitance, Z_c is the characteristic impedance of the transmission line and the input impedance of the processing electronics, and s is the cable attenuation [3]. The I_0 and I_1 terms are the zero- and first-order Bessel functions that describe the low-beam-velocity effects of the beam image-current longitudinal distribution caused by the probe radius, R , and the diffuse beam radius, r , respectively [4].

The measured beam-position and taut-wire probe characterization is the logarithmic ratio (in dB) of the opposite lobe signal amplitudes and may be expressed as

$$R_X(t) = 20 \log \left\{ \frac{1 + \frac{4}{\theta_0} \sum_{n=1}^{\infty} \frac{1}{n} \left(\frac{r_0(t)}{R} \right)^n \cos(n\phi(t)) \sin\left(\frac{n\theta_0}{2}\right)}{1 + \frac{4}{\theta_0} \sum_{m=1}^{\infty} \frac{1}{m} \left(\frac{r_0(t)}{R} \right)^m \cos(m\phi(t)) \sin\left(m\left(\pi + \frac{\theta_0}{2}\right)\right)} \right\}, \quad (4)$$

where $R_X(t)$ is the ratio of the signal amplitudes of opposing lobes, and r_0 and ϕ are the polar coordinates of the beam position [5]. For an "ideal" probe, Equation (4) and its inverse may be reduced with minimal loss of information to include only offsets, first-, and third-order coefficients. This simplification yields a probe/beam position inverse transfer function of

$$x(t) = x_0 + S_1 R_X(t) + S_3 R_X^3(t) + S_5 R_X^5(t) + S_7 R_X^7(t). \quad (5)$$

The S or "sensitivity" terms in Equation (5) are calculated based on two dimensional, third order polynomial least squares fit to the measured characterization map BPM data. This characterization based model provides $\pm 1\%$ accurate beam position measurement inside 30% of the probe radius

(linear portion of a probe) and $\pm 4\%$ accurate beam-position measurements from 30% to 80% of the probe radius [5].

The position processor consists of an amplitude-to-phase converter followed by a phase-detection circuit [2], [6]. The amplitude-to-phase technique converts an input two-port amplitude ratio to a phase difference between output ports using vectorial processing techniques. This phase difference is then detected with a double balanced mixer. The low frequency output of the double balanced mixer is a voltage that is a function of the input signal power ratios. The transfer function describing the position processor is

$$V_{BP}(t) = -\frac{4GA_{rf}}{\pi} \left[\tan^{-1} \left(10^{\frac{R_X(t)}{20}} \right) - \frac{\pi}{4} \right], \quad (6)$$

where $V_{BP}(t)$ is the output voltage, G is the output amplifier gain, and A_{rf} is the peak voltage driving the double balance mixer [6]. Figure 2 shows the Equation (6)-based least-squares fit to the measured values of an AFEL position processor. There is a 3% difference between the fitted equation and measured data when the measured values for the processor constants, G and A_{rf} , were substituted into the fit variable, $\frac{4GA_{rf}}{\pi}$.

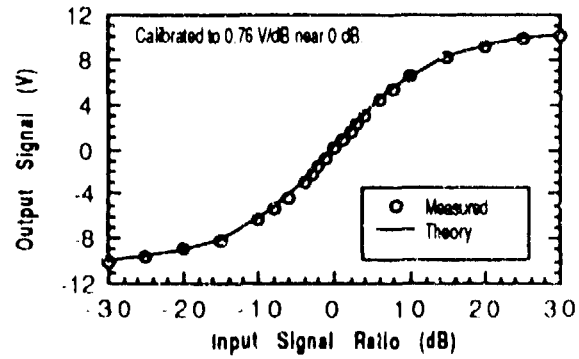


Figure 2. Measured data versus calculated theory [i.e., a least squares fit to Equation (6)] of the beam-position processor transfer function.

The beam intensity measurement system processes the summation of the four lobe signals. It does this by synchronously detecting these summed signals with a double balanced mixer operating as a full-wave detector. The intensity transfer function, $V_I(t)$, is

$$V_I(t) = G_i G_o \frac{3,105}{\pi} i_B(t), \quad (7)$$

where $i_B(t)$ is the average beam current during the macropulse, G_o is the output amplifier gain term, and G_i is the input transconductance gain term that converts the electron beam current to the peak RF input voltage to the double balanced mixer [7].

The control system algorithms use the inversion of Equation (6),

$$R_x(t) = 20 \log \left[\tan \left(\frac{V_{BP}(t)\pi}{4GA_{rf}} + \frac{\pi}{4} \right) \right] \quad (8)$$

and the probe inverse transfer function [Equation (5)] for beam position, and the inversion of Equation (7) for beam intensity [8].

III. BEAM TEST RESULTS

Two beam tests were conducted to verify the operation of the beam position and intensity measurement system. The first test was the measurement of the capacitive-probe frequency response using the AFEL bunched beam. The second test was a position measurement test comparing the beam positions measured by the BPM system and an optical transition radiation (OTR) profile monitor [1].

The signal power model from Equation (3) was calculated based on the actual geometries of the AFEL BPMs. These calculated data were then compared to a set of acquired data (Figure 3) based on an independently measured bunch length and beam current. There is very good agreement between the probe model and measured data up to approximately 2 GHz. Past these frequencies, it is likely this simple model [Equation (3)] does not accurately describe the beam/probe interaction.

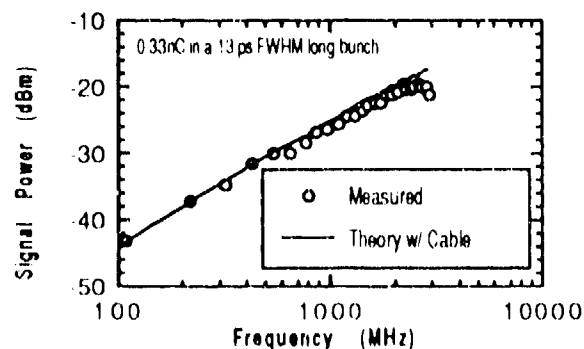


Figure 3. These signal power data are the average of the top and bottom lobes' signal powers as a function of frequency from a centered electron beam. The theoretical model is the calculated signal power based on Equation (3).

The beam position data were acquired by steering the beam in both axes with a dipole magnet upstream of the OTR viewing screen and BPM. The beam positions were then acquired simultaneously with the BPM system and the OTR screen. Figure 4 shows the comparison between the OTR- and BPM-acquired data. There is good agreement between the two measurements in both axes, as can be seen by the 0.02% and 3.1% gain term errors and the -0.164 and 0.245 mm offset errors. The larger vertical offset and gain term errors are most likely caused by the inaccurate angular alignment of the OTR view screen with respect to the vertical axis.

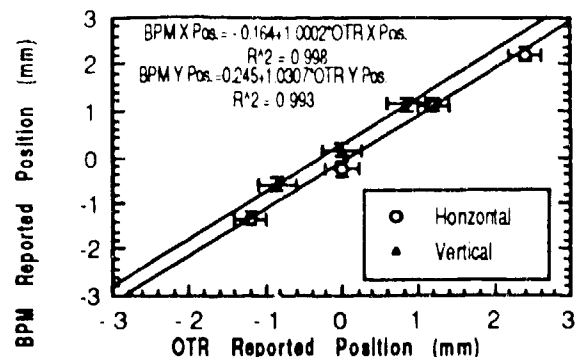


Figure 4. Horizontal and vertical beam position data show correlations between OTR and BPM data. The equations are least squares fit to these data and "R^2" are X^2 values.

IV. CONCLUSION

A series of beam-position and intensity-measurement systems were installed and commissioned on the AFEL beamline. Analytic theoretical transfer functions for each system component were derived, calculated, and measured. There was good agreement between the theoretical component functions and measured system data. Also, beam data were taken and shown to agree with the measurement system models for change in both beam current and beam position. These systems are now operational and are providing valuable information to the AFEL researchers.

VI. REFERENCES

1. K. C. Dominic Chan, et al., "Compact free-electron laser at the Los Alamos National Laboratory," in *SPIE's International Symposium on Optical and Optoelectronic Applied Science and Engineering*, San Diego, CA (1991).
2. J. D. Gilpatrick, et al., "Measurements and Performance of a Microstrip Beam Probe System," in *IEEE Particle Accelerator Conference*, 91CH3038-7, 2, 1136 (1991).
3. J. D. Gilpatrick, et al., "Design and Operation of a Bunched Beam, Phase-Spread Measurement," in the *1992 Linear Accelerator Conference Proceedings*, Vol. 1, pp. 359-361.
4. J. H. Cuperous, "Monitoring of Particle Beam at High Frequencies," *NIM* **145**, 219-231 (1977).
5. J. Power, et al., "Characterization of Beam Position Monitors in Two Dimensions," in the *1992 Linear Accelerator Conference Proceedings*, Vol. 1, pp. 362-365.
6. J. D. Gilpatrick, et al., "Microstrip Probe Electronics," Los Alamos National Laboratory document LA CP 89 488 (1989).
7. J. D. Gilpatrick and E. D. Wells, "Double Balanced Mixer Operation Used as Phase and Synchronous Detector as Applied to Beam Position and Intensity Measurements," Los Alamos National Laboratory document LA UR 93 1622 (1992).
8. J. D. Gilpatrick, "Microstrip Measurement Algorithms," Los Alamos National Laboratory document LA UR 93 1639 (1992).